

Supporting Information for

Understanding Solution State Conformation and Aggregate Structure of Conjugated Polymers via Small Angle X-ray Scattering

Justin J. Kwok^{1*}, Kyung Sun Park², Bijal B. Patel², Rishat Dilmurat³, David Beljonne³, Xiaobing Zuo⁴, Byeongdu Lee⁴ and Ying Diao^{1,2,5,6*}

¹Department of Materials Science and Engineering, University of Illinois at Urbana-Champaign, 1304 W. Green St., Urbana, IL 61801, USA.

²Department of Chemical and Biomolecular Engineering, University of Illinois at Urbana-Champaign, 600 S. Mathews Ave., Urbana, IL 61801, USA.

³Laboratory for Chemistry of Novel Materials, University of Mons, Place du Parc, 20, B-7000 Mons, Belgium.

⁴Advanced Photon Source, Argonne National Laboratory, Lemont, Illinois 60439, USA.

⁵Beckman Institute, Molecular Science and Engineering, University of Illinois at Urbana-Champaign, 405 N. Mathews Ave., Urbana, IL 61801, USA.

⁶Frederick Seitz Materials Research Laboratory, University of Illinois at Urbana-Champaign, 104 S. Goodwin Ave., Urbana, IL 61801, USA

*Co-corresponding authors. Email: jjkwok2@illinois.edu (J.J.K.), yingdiao@illinois.edu (Y.D.)

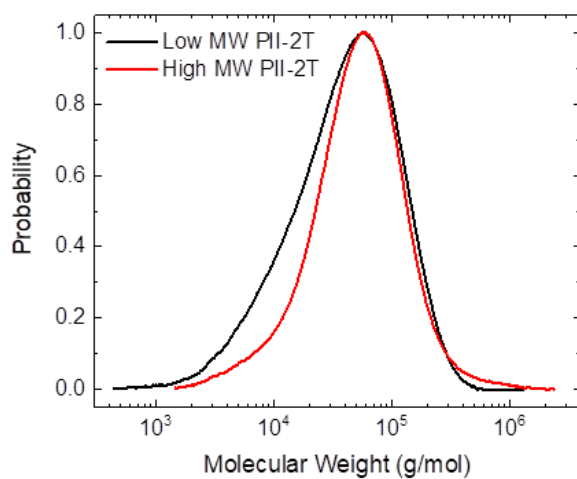


Figure S1. Weight-averaged molecular weight distribution of low and high MW PII-2T

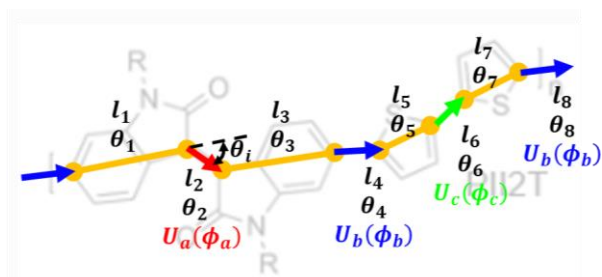


Figure S2. Schematic of segment lengths and angles of the PII-2T repeat unit used for persistence length calculation. The three unique dihedral potentials are indicated in red, green, and blue.

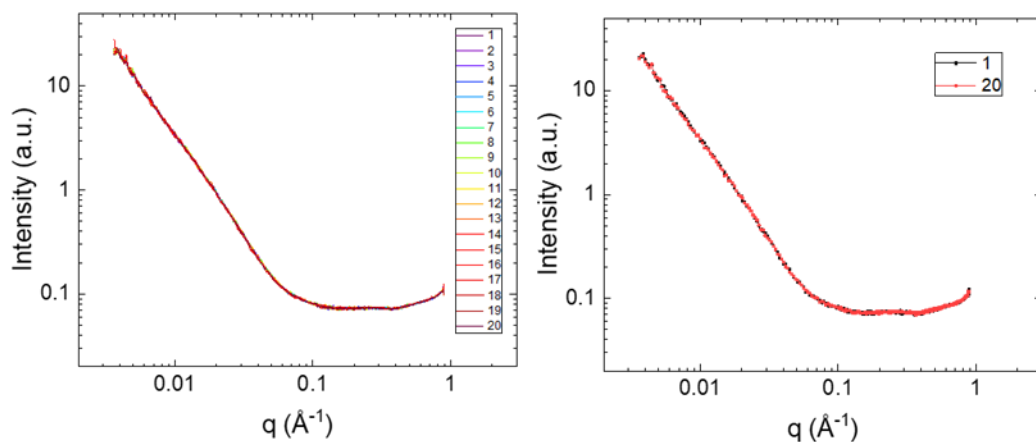


Figure S3. Individual 0.1 s exposure shots of Low MW PII-2T in CB at 10 mg/mL (before background subtraction). All 20 shots are shown in (left) while the first and last shots are shown in (right).

Table S1. Values of segments lengths and angles of the PII-2T repeat unit from DFT used for persistence length calculation. Angles correspond to the angle between the i -th and i -th + 1 segment.

Segment #	1	2	3	4	5	6	7	8
Length, l (Å)	4.26	1.38	4.28	1.46	2.53	1.45	2.52	1.46
Angle, θ (°)	37.7	-37.7	5.10	-14.7	-15.3	15.3	14.7	-5.10

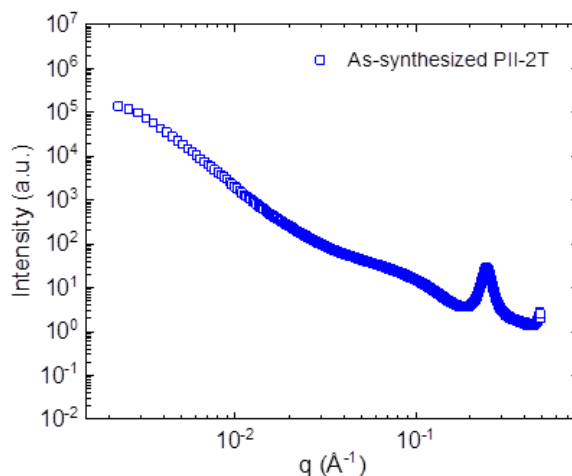


Figure S4. Transmission SAXS of solid as-synthesized PII-2T showing a lamellar peak at $q = 0.25 \text{ \AA}^{-1}$.

Section S1. Discussion of SAXS profiles for varying molecular weight and solvent

As discussed in the main text, we are able to infer the solution state structure by comparing the low/high molecular weight and CB/Dec solvent solutions and show that it is consistent with the picture of two elongated, semiflexible populations corresponding to the fibrillar aggregate and the dispersed polymer chains. The first feature discussed is the drastically different scattering at low q where low MW solutions exhibit a semiflexible power law slope of ~ -1.6 and high MW solutions have a steeper slope of -3.3 . Looking at the low q region of the high MW PII-2T solutions, we see that not only is the slope steeper at -3.3 but the Guinier knee at $q \sim 0.025 \text{ \AA}^{-1}$ is no longer visible. On an initial analysis, one may conclude that the aggregates for high MW PII-2T have become 3-dimensional in shape or that a Guinier knee may be hidden at $q \sim 0.02 \text{ \AA}^{-1}$ at the concave crossover in slope from -3.3 to -1.3 (similar to a Guinier knee for persistence length occurring at a crossover from -2 to -1). However, we conclude that this is not the case on the basis

that a slope of -3 to -4 is indicative of interfacial Porod scattering which in this case indicates that the size of the aggregate is large enough to be outside the experimental q -range. Additionally, while the slope of -3.3 is somewhat close to -3 we note that this is the apparent slope and that since it becomes shallower with increasing q the underlying slope contribution must in fact be steeper than -3.3 , and is in fact closer to -4 as shown by the model fitting. Because the low q scattering is due to Porod scattering, the crossover in slope from -3.3 to -1.3 at $q \sim 0.02 \text{ \AA}^{-1}$ is not due to a hierarchical structural change within a single particle but instead must be a result of the summation of two separate, independent contributions (the fibril aggregate and the dispersed polymer). This is in agreement with our previous conclusion that the high q and low q scattering features correspond to separate aggregate and polymer contributions. Additionally, the presence of Porod scattering and the disappearance of the Guinier knee at $q \sim 0.025 \text{ \AA}^{-1}$ both point towards the notion that this Guinier does in fact correspond to the fibril aggregate and that it has likely shifted to the left outside the q -range indicating the aggregates are simply larger for high MW PII-2T. This explanation is more plausible and also highly consistent with our imaging results. Finally, as a consequence of the aggregate Guinier knee shifting out of the q -range, scattering from the polymer contribution at intermediate q (0.03 to 0.1 \AA^{-1}) is no longer hidden and exhibits a power law slope of -1.3 which further confirms the idea that the high q Guinier knee corresponds to the cross-section of a semiflexible polymer. In fact, the scattering profiles for high MW PII-2T are nearly identical in CB and Dec now that aggregate scattering is out of the q -range and the polymer scattering is more visible, with the only difference being the lamellar peak in CB.

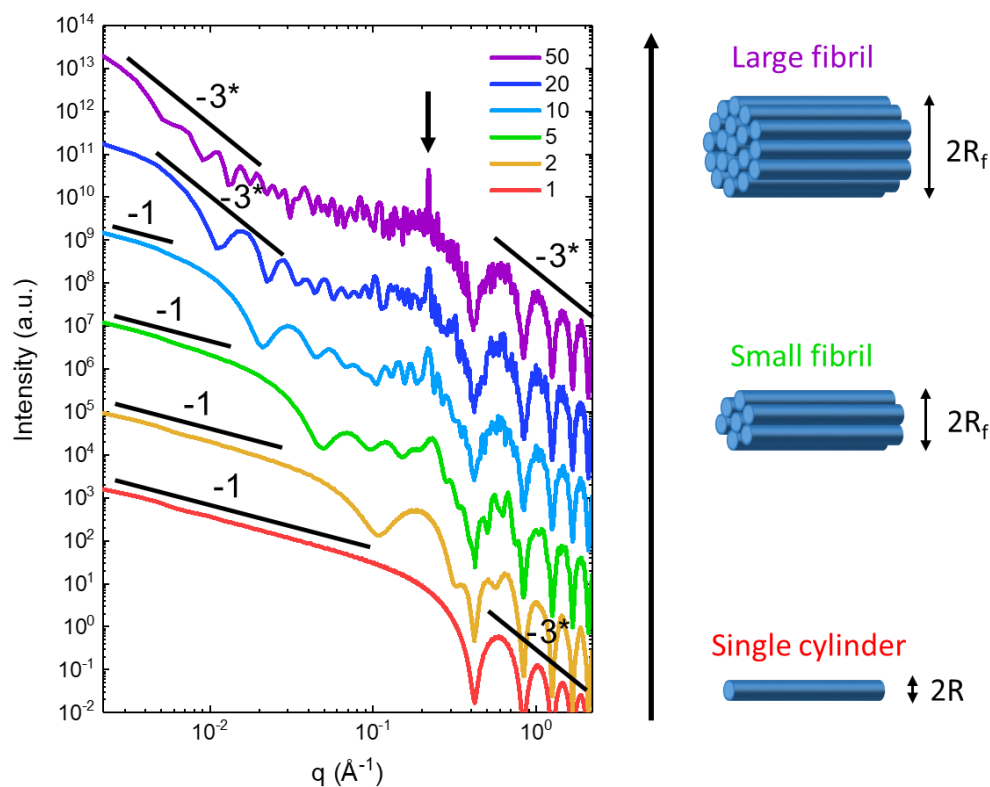


Figure S5. Simulated scattering intensity of fibrils formed by 2D cylinder bundling with increasing diameter. The scattering profile ranges from a single cylinder (red) to a large fibril aggregate consisting of 50 cylinders (purple). The number of cylinders is indicated by the legend. As the fibril diameter increases the cross-sectional Guinier knee shifts to lower q until it is out of range and only contributes its trailing Porod region at low q . A structure factor peak emerges (indicated by arrow) as the cylinders aggregate as well. The length of the cylinders is larger than the fibril radius and its corresponding Guinier knee is out of range in all cases. *Note that due to the 2D nature of the simulation the power law slope of the Porod scattering is -3 . For a real 3D system the power law slope would instead be ideally -4 .

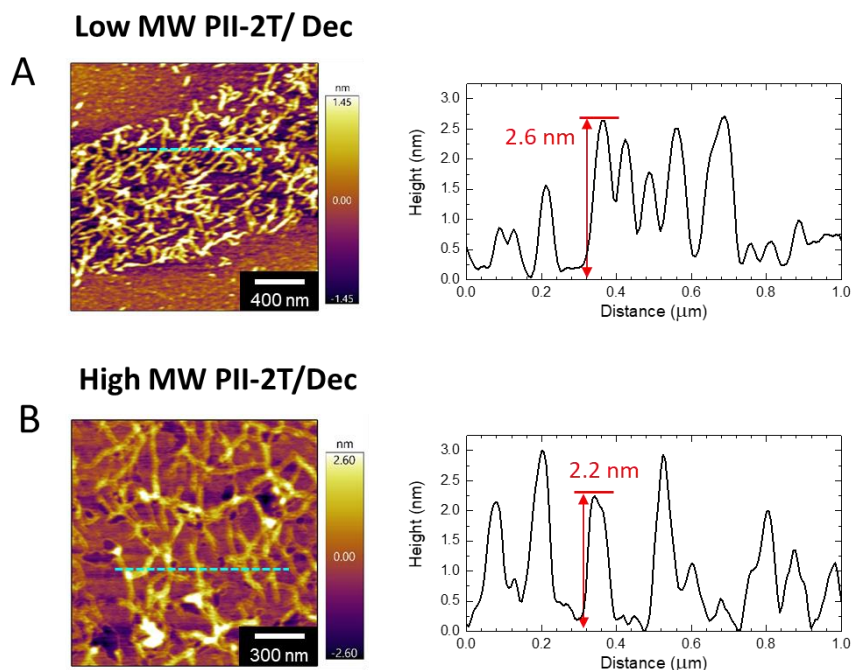


Figure S6. AFM imaging of freeze dried (A) low and (B) high MW PII-2T from Dec. AFM linecuts (right) show that despite these features having widths of several 10's of nm, the heights are consistently ~ 2.5 nm corresponding to a single lamella. These features are therefore ribbon-like but are believe to be formed during the freeze-drying solution preparation as discussed below.

Section S2. Discussion of ribbon-like features in freeze-dried imaging of PII-2T in Dec

From our initial analysis of the scattering data we surmised that there exists two populations of scatterers, corresponding to an aggregate and dispersed polymer population, both of which appear to be elongated, semiflexible objects. Considering the imaging data, we can clearly see the presence of fibril aggregates in both CB and Dec as well as further agglomeration in Dec. These objects account for the low q scattering features. What is interesting however is that we also observe elongated objects with AFM heights of ~ 2.5 nm and widths of approximately 50 nm. One notes that that this height of 2.5 nm is the same as both the lamellar stacking distance and the polymer diameter. Thus it appears these objects are ribbon-like consisting of pi-pi stacking to

form a single lamella for its cross-section. From our initial analysis and discussion in the main text we were able to infer the existence of the dispersed polymer population based on the fact that a cross-sectional Guinier knee existed at high- q corresponding to ~ 2.5 nm with a power law slope of -1.3 preceding it in high MW data. Therefore, the existence of these ribbon-like objects gives rise to the questions: Does this cross-sectional Guinier knee that we previously ascribed to the dispersed polymer with a diameter 2.5 nm instead correspond to ribbon-like object with a single lamella thickness of 2.5 nm? And if not, why are they not reflected in the scattering profile? And do they really exist in solution?

First, we address the initial question. Asking whether the high q Guinier knee corresponds to the dispersed polymer or the ribbon-like objects is similar to asking whether the knee corresponds to a small isotropic cross-section (2.5 nm) or the minor axis of a highly anisotropic cross-section (2.5 nm by 50 nm). Considering that the length is larger than the cross-sectional dimensions in both cases, one can see that the power law slope preceding the cross-sectional Guinier knee can be as shallow as -1 for the isotropic cross-section (as it can appear rod-like at length-scales just above the 2.5 nm diameter), but the power slope can only be as shallow as -2 for the highly anisotropic cross-section (as the ribbon object appears plate-like at length-scales just above the 2.5 nm minor diameter but below the 50 nm major diameter). This can also be seen quantitatively based on the calculated form factor of an elongated elliptical cylinder or an elongated parallelepiped having a cross-sectional axis ratio of 1 in the first case and a high ratio of 50/2.5 in the second case. Given that the experimental data shows that the power law just preceding the 2.5 nm knee has a slope of -1.3 it is impossible for this knee to correspond to the minor axis of a highly anisotropic cross-section and therefore the slope of -1.3 is much more reasonably ascribed to the semiflexibility of an elongated object with a cross-sectional aspect ratio closer to 1

(i.e. the dispersed polymer chains). This therefore affirms the picture we developed consisting of fibril aggregates and dispersed polymer chains which is accurate for CB and still applicable for Dec cases.

The next questions are then why do these ribbons not contribute to scattering in Dec cases and if they really exist in solution. Naturally, if these ribbon features do not exist in solution and are instead an artifact of the freeze-dried imaging process then they would not contribute to the solution scattering. We do not yet have a firm answer to these questions and this subject is of interest in our follow up works focusing on the solvent effect of D-A polymer scattering. Despite this, we do note several observations about the ribbon-like objects that brings their existence in the solution state into question. First, consider that during the freeze drying process one would expect that these ribbons exist in the 3D solution volume at random orientations (both the orientation of the long axis and the orientation rotating around the long axis) and then fall onto the substrate surface as the frozen decane is sublimated. One would then expect that when imaging the surface we would see 1) that the ribbons were frozen are different orientations around its long axis such that when fallen upon the substrate the measured heights of various ribbons ranges from the minor diameter to the major diameter (2.5 nm laying flat to 50 nm on its side) and 2) that we would observe overlapping of the ribbons producing nodes where the local thickness is 2 or more ribbons tall which should yield localized heights of 5+ nm in the case of overlapping ribbons both laying flat to ~100+ nm in the case of overlapping ribbons both on their sides. From our imaging of both low and high MW PII-2T in Dec we observe that both of these assertions are false as the peak heights are consistently around 2.5 nm at most, never approaching the major diameter of ~50 nm, and that even in regions where it appears that ribbons are overlapping the measured height is still around 2.5 nm. These observations are inconsistent with the idea that these ribbons exist in the

solution state but are instead highly suggestive of surface-induced growth or adsorption of the polymers to the surface during solution preparation. Furthermore, we have observed these ribbon-like features in conjugated polymers solutions with other chlorinated solvents as well indicating it is not specific to Dec and appears to be present due to the sample preparation.

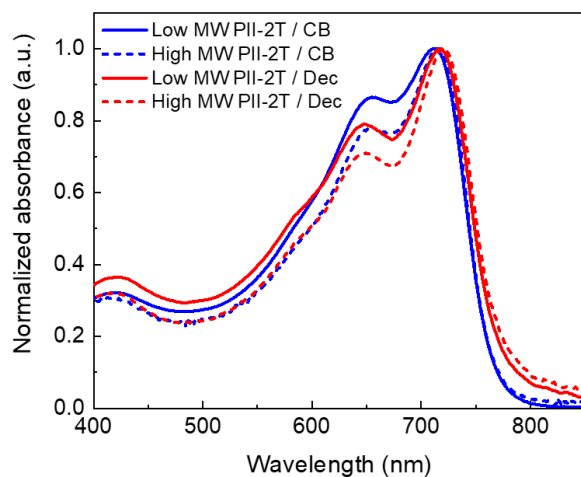


Figure S7. Normalized UV-Vis spectroscopy of low and high MW PII-2T solutions in CB and Dec.

Section S3. SAXS theory

As a basis for our models we describe here the general theory for scattering of particle assemblies.

The absolute scattering intensity for a dilute solution is

$$\frac{d\Sigma}{d\Omega}(q) = \frac{N_{agg}}{V} I(q)$$

where N_{agg} is the number of aggregates and V is the volume of the solution. We refer to the scattering intensity as $I(q)$ as absolute intensity calibration is not carried out in this work. Ideally, a solution of dispersed particles has a scattering intensity of

$$I(q) = NP(q)S(q)$$

where N is the number of primary particles within an aggregate, $P(q)$ is the primary particle form factor and $S(q)$ is the structure factor. In this work we define the form factor as $P(q) = \Delta\rho^2 V^2 \Sigma(q)$ where $\Delta\rho^2$ is the contrast and $\Sigma(q)$ is the shape function of the scattering particle such that $\Sigma(q = 0) = 1$ (in other works this is sometimes referred to as the form factor instead). The scattering amplitude of the particle is

$$F(q) = \int_V \Delta\rho(r) e^{-iqr} dr$$

Therefore, in this work the form factor is $P(q) = |F(q)|^2$ and the shape function is $\Sigma(q) = (|\int_V e^{-iqr} dr|/V)^2$.

Typically, a solution of homogeneously dispersed primary particles has an excess SLD of $\Delta\rho = \rho_{pp}(r) - \rho_{solv}$ where $\rho_{pp}(r)$ is the SLD of the primary particle and ρ_{solv} is the mean SLD

of the solution which corresponds to the solvent for dilute solutions. The scattered intensity is then $I(q) = NP(q)S(q)$ where N is the number of particles and $S(q)$ is the structure factor. As shown in ref²⁴ if instead the primary particles assemble into aggregates, then an equivalent expression for the excess SLD shown above is $\Delta\rho = \rho_{pp}(r) - \rho_{agg}(r) + \rho_{agg}(r) - \rho_{solv}$ where $\rho_{agg}(r)$ is the mean SLD of the aggregate. The first two terms represent the excess SLD of polymers within the aggregate $\Delta\rho_{pp} = \rho_{pp}(r) - \rho_{agg}(r)$ and the last two terms represent the excess SLD of fibers in solvent $\Delta\rho_{agg} = \rho_{agg}(r) - \rho_{solv}$. Although the aggregate is composed of the primary particle the SLD's can differ due to differences in local density as well as interpenetration of solvent molecules in the aggregate structure. By means of the autocorrelation approach with the excess SLD the scattering intensity is then²⁴

$$I(q) = N_{pp}P_{pp}(q)S_{\infty}(q) * \Sigma'_{agg} + P'_{agg}(q)$$

where the first term resembles the non-aggregated result but only pertains to the primary particles within the aggregate such that N_{pp} is the number of primary particles within the aggregate, $S_{\infty}(q)$ is the structure factor of the primary particles within an infinite domain, and $*$ represents the convolution operation. The second term corresponds to the aggregate where $P'(q)$ denotes the form factor corresponds to the external shape without regard for internal structure. In the scattering amplitude approach this term derives from convolution of the form factor with the null scattering term that is typically neglected. The scattering intensity can be reduced and rewritten as

$$I(q) = N_{pp}P_{pp}(q) \left[\frac{\Delta\rho_{agg}^2}{\Delta\rho_{pp}^2} N_{pp}\Sigma'_{agg} + S_{\infty}(q) \right]$$

We then apply this to describe the aggregated cross-section of the fibril consisting of polymer chain cross-sections. In this case, $P_{pp}(q)$ corresponds to the elliptical cross-section of the

aggregated polymer and Σ'_{agg} corresponds to the circular cross-section of the fibril. The elliptical cross-section has the shape function

$$\Sigma_{CS,i}(q; R_i) = \int_0^{\frac{\pi}{2}} \left[\frac{2J_1(qR_i)}{qR_i} \right]^2 d\theta$$

where $J_1(x)$ is the first-order Bessel function and $R_i = (r_{maj}^2 \varepsilon^2 \sin^2 \theta + r_{maj}^2 \cos^2 \theta)^{1/2}$ with r_{maj} as the major radius and $\varepsilon = r_{min}/r_{maj}$ as the ratio of the minor radius to the major radius. For a circular cross-section, the radius is constant and so the shape function simply becomes $[2J_1(qR)/(qR)]^2$. The aggregated cross-section is then multiplied by the semiflexible axial shape function. Strictly speaking the shape function of elongated objects comes from orientational integration of cross-sectional and axial terms coupled together. However, in the case where the length of the object is much larger than its diameter the function can be decoupled into a product of its cross-sectional and axial terms³⁵. The result is then the first term of equation (5) in the main text. One can also use a rectangular cross-section for a semiflexible parallelepiped which should yield similar results to the semiflexible elliptical cylinder.

For the 2SFC model, a pseudo-Voigt peak function $V_P(q)$ is used to capture the high- q structure factor peak. The pseudo-Voigt peak is a linear combination of a Gaussian and Lorentzian given by the following equation.

$$V_P(q) = \mu \frac{2}{\pi} \frac{w}{4(q - q_c)^2 + w^2} + (1 - \mu) \sqrt{\frac{4 \ln 2}{\pi}} \frac{1}{w} e^{-4 \ln 2 \frac{(q - q_c)^2}{w^2}}$$

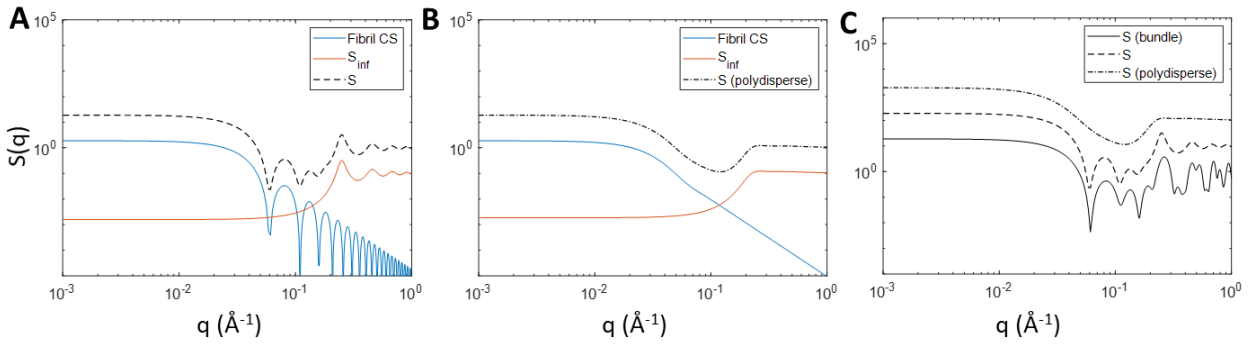


Figure S8. Comparison between structure factors for cross-sectional aggregation within fibrils. Structure factor calculated using the particle assembly theory used in this work for a cross-section consisting of (A) 19 monodisperse cylinders of $R = 14 \text{ \AA}$ with $\phi_{HS} = 0.5$ and (B) 19 polydisperse cylinders of $\bar{R} = 14 \text{ \AA}$ and $\sigma = 0.3$ with $\phi_{HS} = 0.6$. The external fibril cross-section and internal structure factor contributions are shown in blue and red, respectively, and are shifted down by 1 decade. The overall structure factor is shown in black. (C) Structure factor for an explicitly positioned bundle of 19 hexagonally close-packed monodisperse cylinders of $R = 14 \text{ \AA}$ (solid line) compared to the monodisperse (dash) and polydisperse (dash-dot) structure factors from A and B. Each curve is shifted by a decade.

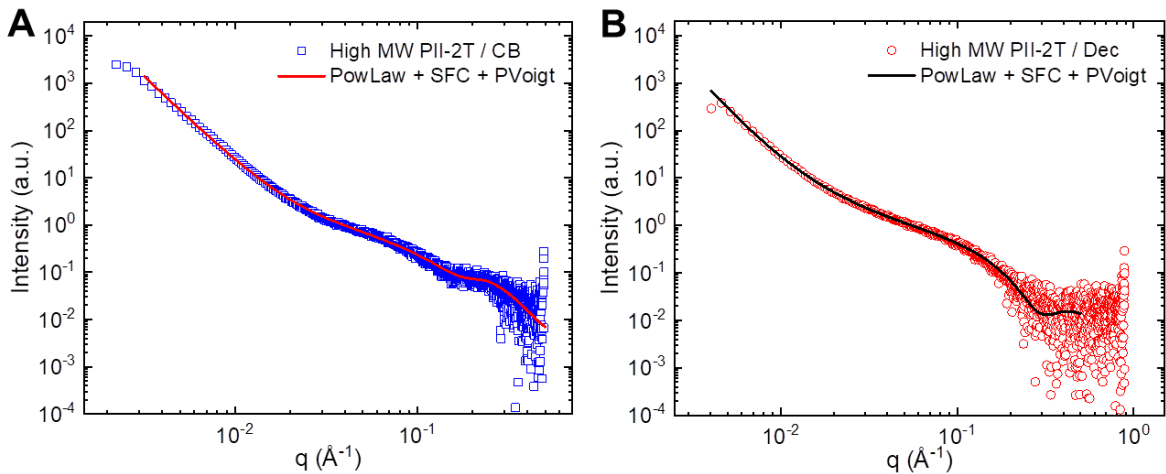


Figure S9. SFC fits using a power law contribution for low q and a pseudo-Voigt peak for high q applied to High MW PII-2T in (A) CB and (B) Dec.

Table S2. Fit parameters for Power Law + SFC + PseudoVoigt model.

Sample	L_p (nm)	$l_{p,p}$ (nm)	R_p (Å)	d	q_c	w	μ
High MW PII-2T / CB	100*	8 ± 1	15.1 ± 0.3	3.77 ± 0.06	0.221 ± 0.005	0.189 ± 0.009	1
High MW PII-2T / Dec	100*	7.6 ± 0.9	11.9 ± 0.2	3.9 ± 0.1	-	-	-

*Values were fixed during fitting.

Table S3. Fit parameters for 2SFC model for Low MW PII-2T CB/Dec series.

Sample	L_f (nm)	b_f	R_f	σ_f	L_p (nm)	$l_{p,p}$ (nm)	R_p (Å)	q_c	w	μ
Low MW PII-2T CB	500*	30.2 ± 8.6	41.2 ± 7.3	0.688 ± 0.17	100*	7.5*	17.0 ± 4.1	0.22 ± 0.02	0.18 ± 0.01	1
Low MW PII-2T CB 80%	500*	>R_f	3.0	0.060	100*	7.5*	2.4	0.19 ± 0.02	0.22 ± 0.01	1
Low MW PII-2T CB 60%	500*	>R_f	53.6 ± 2.7	0.317 ± 0.058	100*	7.5*	14.9 ± 1.2	0.19 ± 0.01	0.15 ± 0.01	1
Low MW PII-2T CB 40%	500*	29.0 ± 8.7	48.2 ± 2.7	0.538 ± 0.074	100*	7.5*	11.7 ± 0.50	0.24 ± 0.01	0.20 ± 0.03	1
Low MW PII-2T CB 20%	500*	13.9 ± 12	46.4 ± 6.4	0.803 ± 0.32	100*	7.5*	12.3 ± 0.17	-	-	-
Low MW PII-2T CB 10%	500*	17.0 ± 2.1	36.1 ± 2.5	0.649 ± 0.077	100*	7.5*	12.6 ± 0.15	-	-	-
Low MW PII-2T Dec	500*	13.3 ± 4.0	40.8 ± 6.6	0.580 ± 0.19	100*	7.5*	12.1 ± 0.59	-	-	-

*Values were fixed during fitting.

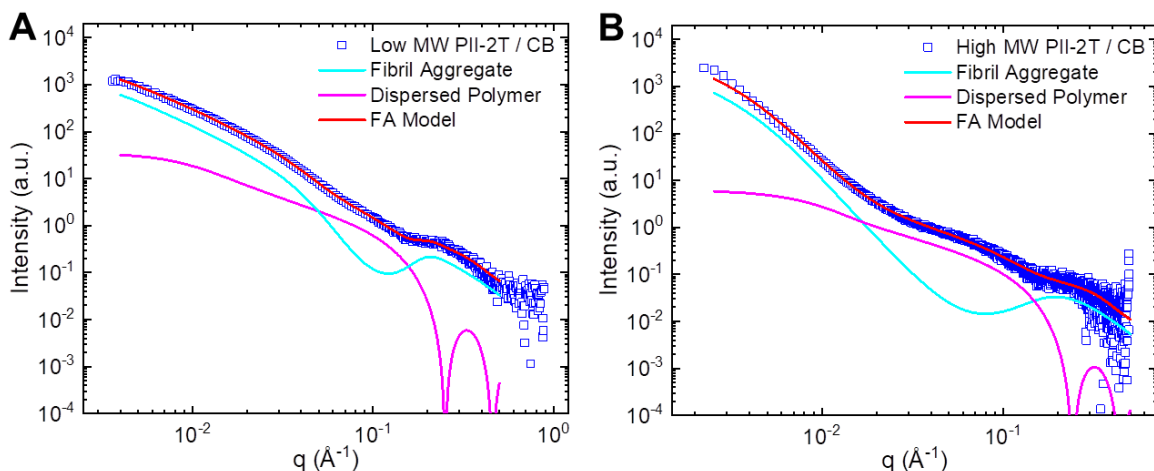


Figure S10. FA model fits to (A) Low and (B) High MW PII-2T in CB with the cross-sectional ellipse axis ratio fixed to 0.13 for the aggregated polymer in order to match the polymer minor diameter to ~ 4 Å corresponding to the pi-pi stacking distance.

Table S4. Fit parameters for the FA model with ellipse axis ratio fixed to 0.13.

Sample	L_f (nm)	$l_{p,f}$ (nm)	ε	N_p/ϕ_p	$\bar{R}_f = (\varepsilon R_p^2 N_p / \phi_p)^{\frac{1}{2}}$ (nm)	L_p (nm)	$l_{p,p}$ (nm)	\bar{R}_p (Å)	σ_p	ϕ_{HS}	γN
Low MW PII-2T / CB	500*	8.5 ± 0.5	0.13*	$80. \pm 3$	4.9 ± 0.1	100*	7.5	15.3 ± 0.3	0.36 ± 0.01	0.63 ± 0.01	5.3 ± 0.2
High MW PII-2T / CB	500*	$>R_f$	0.13*	3900 ± 300	36 ± 2	100*	4	15.9 ± 0.4	0.51 ± 0.04	0.69 ± 0.02	91 ± 8

*Values were fixed during fitting.

Table S5. Fitting parameters for FA model fits to various different conjugated polymer systems.

Sample	L_f (nm)	$l_{p,f}$ (nm)	ε	N_p/ϕ_p	$\bar{R}_f = (\varepsilon R_p^2 N_p / \phi_p)^{\frac{1}{2}}$ (nm)	L_p (nm)	$l_{p,p}$ (nm)	\bar{R}_p (Å)	σ_p	ϕ_{HS}	γN
PIII-2T / CB	500*	$>R_f$	0.16 ± 0.02	1400 ± 300	33 ± 4	100*	$>R_p$	22.1 ± 0.2	0.50 ± 0.01	0.80 ± 0.01	8 ± 2
DPP2T-TT / CB	500*	$>R_f$	0.33 ± 0.03	400 ± 200	22 ± 4	15.5 ± 0.8	9 ± 2	18.5 ± 0.6	0.66 ± 0.03	0.82 ± 0.01	1.1 ± 0.6
DPP-BTz / CB	500*	$>R_f$	0.35 ± 0.02	10 ± 4	3 ± 1	-	-	16.2 ± 0.6	0.49 ± 0.07	0.75 ± 0.05	0.2 ± 0.2
PDPP2FT-C ₁₆ / CB	500*	$>R_f$	0.30	400	18	100*	20.	17.2	0.54	0.74	1.2
P3HT- <i>b</i> -DPPT- T / DCB	500*	$>R_f$	0.29	1700	30.	100*	4.7	13.5	0.31	0.999	1e-5
P(NDI2OD-T2) / DCB	500*	$>R_f$	0.15	5	1.3	-	-	15.4	0.34	0.82	0.031

*Value was fixed during fitting.

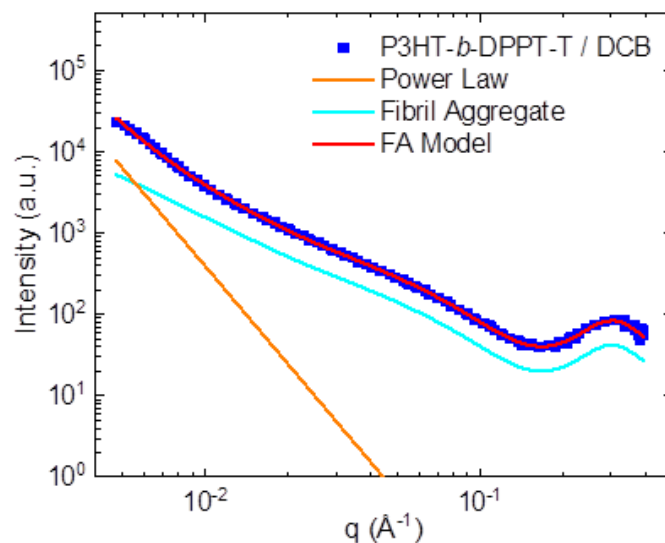


Figure S11. Alternative fibril aggregate model of P3HT-*b*-DPPT-T in DCB where the intermediate Guinier knee corresponds to the aggregate instead of the separate polymer chains. A power law of -4 corresponding to larger agglomerate Porod scattering is added to fit the low q region.

Table S6. Fit parameters for the alternative fit to P3HT-*b*-DPPT-T in DCB.

Sample	L_f (nm)	$l_{p,f}$ (nm)	ε	N_p/ϕ_p	$\bar{R}_f = (\varepsilon R_p^2 N_p / \phi_p)^{\frac{1}{2}}$ (nm)	L_p (nm)	$l_{p,p}$ (nm)	\bar{R}_p (Å)	σ_p	ϕ_{HS}	γN
P3HT- <i>b</i> -DPPT-T / DCB	500*	8.12	0.198	15.8	1.62	-	-	9.15	0.343	0.508	0.218

*Values were fixed during fitting